Journal of Molecular Spectroscopy 282 (2012) 34–38

Contents lists available at SciVerse ScienceDirect

Journal of Molecular Spectroscopy

journal homepage: www.elsevier.com/locate/jms

Additional bands of the Ar–D_2O intramolecular bending mode observed using a quantum cascade laser

Jacob T. Stewart [a], Benjamin J. McCall [b,*]

[a] Department of Chemistry, University of Illinois, 600 South Mathews Avenue, Urbana, IL 61801, USA
[b] Departments of Chemistry and Astronomy, University of Illinois, Urbana, IL 61801, USA

ARTICLE INFO

Article history:
Received 9 October 2012
In revised form 13 November 2012
Available online 29 November 2012

Keywords:
Van der Waals complex
Water clusters
Quantum cascade laser

ABSTRACT

Three new rovibrational bands of Ar–D_2O have been observed in the ν_2 bending region of D_2O using a quantum cascade laser based cavity ringdown spectrometer. In addition, further observations of the $\Pi(1_{10}, \nu_2 = 1) \leftarrow \Sigma(1_{01})$ band reported by Li et al. (J. Mol. Spectrosc. 272 (2012) 27–31) have been made. All bands were fit by treating the complex using a pseudo-diatomic model which treats the D_2O as a free rotor within the complex. Molecular constants have been obtained using this model and are reported with deviations in the fits ranging from 0.0002 cm^{-1} to 0.0005 cm^{-1}. Two of the newly observed bands are tentatively assigned as the $\Pi(2_{02}, \nu_2 = 1) \leftarrow \Sigma(1_{11})$ and $\Pi(2_{11}, \nu_2 = 1) \leftarrow \Sigma(2_{02})$ bands, which have not previously been observed in other spectral regions.

1. Introduction

The interaction of water with itself and other molecules plays a key role in many diverse chemical environments, such as biochemical systems and solution phase chemistry. Because of the importance of these interactions, much work has been devoted to gaining a detailed understanding of them through simple model systems such as rare gas–water clusters. In particular, Ar–H_2O and Ar–D_2O have been extensively studied through high-resolution microwave [1,2], far-infrared [3–7], and infrared [8–12] spectroscopy. This work has shown that the water molecule acts as a nearly free rotor within the Ar–water complex. The data from these spectroscopic studies were used by Cohen and Saykally to generate an empirical intermolecular potential energy surface for the Ar–water complex [13]. More recently, Makarewicz has generated an *ab initio* potential energy surface for various rare gas–water complexes, including Ar–H_2O [14].

In this article, we present rovibrational spectra of Ar–D_2O in the region of the ν_2 bending mode of D_2O, which expands on the previous work of Li et al. [12] who recently reported three rovibrational bands of Ar–D_2O in this region. In the present work, we provide additional data for one of these previously observed bands and also report three new bands which have not previously been observed.

2. Experimental

Our quantum cascade laser (QCL) spectrometer has been described in detail previously [15,16], but we briefly summarize the instrument here. We generate mid-IR light using a liquid nitrogen cooled Fabry–Perot QCL provided by the Gmachl group at Princeton. By varying the temperature and current applied to the QCL, the frequency can be tuned from ~1180–1200 cm^{-1}, allowing us to observe the strongest bands of Ar–D_2O. The light is sent to an optical cavity, where we perform continuous wave cavity ringdown spectroscopy (cw-CRDS) to obtain an absorption spectrum of the clusters. We calibrate the frequency of our laser using a mid-IR wavemeter (Bristol) and SO_2 absorption lines contained in the HITRAN database [17]. We estimate that our absolute frequency accuracy is ~0.0005 cm^{-1} (15 MHz).

Ar–D_2O clusters are generated by bubbling Ar through room temperature D_2O (Cambridge Isotope Laboratories) and then expanding the gas mixture through a 150 μm × 1.2 cm slit to generate a continuous supersonic expansion. The flow rate of Ar through the system was controlled by a mass flow controller (MKS Instruments). The backing pressure behind the nozzle was measured using a pressure gauge on the input line into the vacuum chamber and typically ranged from 300–400 Torr, though some data were acquired using backing pressures up to ~700 Torr. The vacuum chamber was pumped by a Roots blower and rotary vane pump (Oerlikon-Leybold). While the gas was flowing, the background pressure in the chamber was measured to range from 100–175 mTorr.

3. Results and discussion

In the frequency region from 1180–1200 cm^{-1} we have observed six rovibrational bands of Ar–D_2O, three of which have been previously reported and analyzed by Li et al. [12]. Here we

* Corresponding author. Fax: +1 217 244 3186.
E-mail address: bjmccall@illinois.edu (B.J. McCall).

0022-2852/$ - see front matter © 2012 Elsevier Inc. All rights reserved.
http://dx.doi.org/10.1016/j.jms.2012.11.002

present additional data for the $\Pi(1_{10},\ v_2 = 1) \leftarrow \Sigma(1_{01})$ band observed by Li et al. [12] near 1193 cm^{-1} and for three additional bands which have not previously been reported.

All bands were fit using PGOPHER [18] by treating Ar–D_2O as a pseudo-diatomic system, similar to Li et al. [12] and Zwart and Meerts [7]. The energy levels for all observed bands are expressed as

$$E(J) = v + BJ(J+1) - D(J(J+1))^2 + \cdots \quad (1)$$

where v is the band origin, B is an effective rotational constant, and D is the effective quartic distortion constant. Fitting of all bands was complicated by the presence of Coriolis coupling between states with the same symmetry (e or f) and internal rotor state [10]. As an example, the $\Pi(1_{10},\ v_2 = 1)$ state is actually comprised of two degenerate states with different symmetry, which we can label $\Pi^e(1_{10},\ v_2 = 1)$ and $\Pi^f(1_{10},\ v_2 = 1)$. The $\Pi^f(1_{10},\ v_2 = 1)$ state participates in Coriolis coupling with the $\Sigma^f(1_{10},\ v_2 = 1)$ state, which lifts the degeneracy. Due to selection rules based on the symmetry of the states [19], Q-branch transitions only occur between states with different symmetry ($f \leftarrow e$ or $e \leftarrow f$) and P- and R-branch transitions only occur between states of the same symmetry ($e \leftarrow e$ or $f \leftarrow f$). Because we do not have data on the $\Sigma^f(1_{10},\ v_2 = 1)$ state, we can only incorporate the effects of the Coriolis coupling into an effective rotational constant and fit the Q-branch separately from the P- and R-branches, which was also the approach taken by Li et al. [12]. We follow this approach and report effective rotational constants for each symmetry state contained in a Π internal rotor state.

3.1. $\Pi(1_{10},\ v_2 = 1) \leftarrow \Sigma(1_{01})$ band

As observed by Li et al. [12] the strongest rovibrational band of *para* Ar–D_2O is the $\Pi(1_{10},\ v_2 = 1) \leftarrow \Sigma(1_{01})$ band found near 1193 cm^{-1}. We have also observed this band and have been able to measure additional transitions beyond what Li et al. were able to obtain with their instrument. Fig. 1 shows the Q-branch region of this band, along with the first few transitions of the P- and R-branches. R-branch transitions from additional $\Pi \leftarrow \Sigma$ bands can also be seen which were not observed by Li et al.

We have fit the band using the approach outlined above, while fixing the constants for the $\Sigma(1_{01})$ state to the values presented in

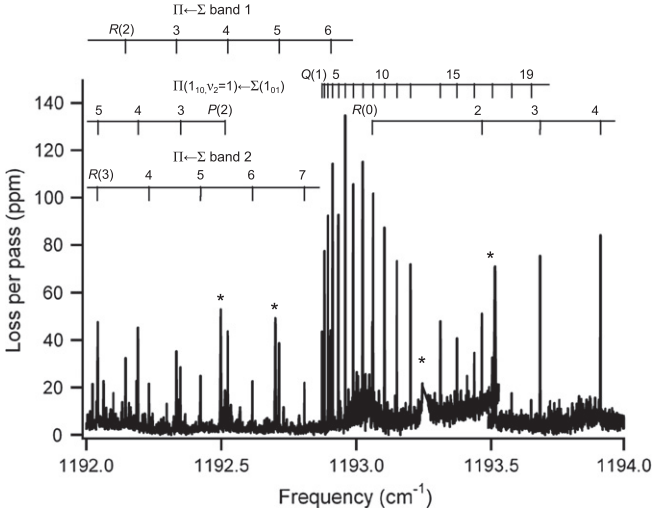

Fig. 1. Q-branch region of the $\Pi(1_{10},\ v_2 = 1) \leftarrow \Sigma(1_{01})$ band, along with the beginning of the P- and R-branches. Additional lines are present from previously unobserved $\Pi \leftarrow \Sigma$ bands. Lines marked with an asterisk (*) are due to D_2O and HOD monomer. The very strong D_2O line near 1193.25 cm^{-1} has been removed for clarity. Other lines are due to $(D_2O)_n$ clusters. The spectrum was collected at a backing pressure of ~300 Torr.

Table 1
Comparison of molecular constants (in cm^{-1}) for the $\Pi(1_{10},\ v_2 = 1) \leftarrow \Sigma(1_{01})$ band reported by Li et al. [12] and the present work. Values in parentheses represent one standard deviation from the least squares fit to the data.

Parameter	Li et al. [12]	Present work
B''	0.09103344(33)[a]	
$D''(\times 10^6)$	1.7666(80)[a]	
v	1192.86911(21)	1192.86863(25)
$B'(e)$	0.095237(20)	0.0952486(40)
$D'(e)(\times 10^6)$	2.01(30)	2.152(14)
$B'(f)$	0.0931767(63)	0.0932128(39)
$D'(f)(\times 10^6)$	1.857(33)	2.101(11)
σ	0.0004	0.0005

[a] From Ref. [7].

Table 2
Observed transitions for the $\Pi(1_{10},\ v_2 = 1) \leftarrow \Sigma(1_{01})$ band (in cm^{-1}). Values in parentheses are residuals (observed – calculated) from the least squares fit.

Transition	Frequency
$P(12)$	1191.2468(11)
$P(11)$	1191.3351(8)
$P(10)$	1191.4317(4)
$P(9)$	1191.5364(−2)
$P(8)$	1191.6497(−8)
$P(7)$	1191.7727(−2)
$P(6)$	1191.9036(−2)
$P(5)$	1192.0424(−10)
$P(4)$	1192.1915(1)
$P(3)$	1192.3479(0)
$P(2)$	1192.5133(4)
$Q(1)$	1192.8734(4)
$Q(2)$	1192.8822(5)
$Q(3)$	1192.8950(3)
$Q(4)$	1192.9121(0)
$Q(5)$	1192.9335(−2)
$Q(6)$	1192.9592(−4)
$Q(7)$	1192.9888(−8)
$Q(8)$	1193.0231(−7)
$Q(9)$	1193.0625(4)
$Q(10)$	1193.1047(3)
$Q(11)$	1193.1504(0)
$Q(12)$	1193.2004(−1)
$Q(14)$	1193.3113(−2)
$Q(15)$	1193.3728(4)
$Q(16)$	1193.4371(4)
$Q(17)$	1193.5042(0)
$Q(18)$	1193.5751(3)
$Q(19)$	1193.6481(−4)
$R(0)$	1193.0596(5)
$R(2)$	1193.4652(0)
$R(3)$	1193.6809(3)
$R(4)$	1193.9049(7)
$R(5)$	1194.1355(−4)
$R(6)$	1194.3753(−2)
$R(7)$	1194.6227(−4)
$R(8)$	1194.8789(6)
$R(9)$	1195.1413(0)
$R(10)$	1195.4100(−16)
$R(11)$	1195.6893(−1)
$R(12)$	1195.9746(2)
$R(13)$	1196.2664(0)
$R(14)$	1196.5652(0)
$R(15)$	1196.8710(3)
$R(16)$	1197.1826(−3)

Ref. [7]. The results of the fit are listed in Table 1 along with the previous results from Li et al. As can be seen in Table 1 our results differ from those obtained by Li et al. for the f state, which corresponds to the observed Q-branch transitions. The constants obtained by Li et al. fit well to the low J Q-branch transitions, which were observed by Li et al. but at higher J values ($\geqslant 14$), the fit

diverges significantly. Because we were able to observe lines up to Q (19), we were able to more accurately determine the constants for the f state, which fit both the low and high J transitions. A list of the observed transitions is presented in Table 2.

3.2. $\Pi(1_{01}, v_2 = 1) \leftarrow \Sigma(1_{01})$ band

We observed a much weaker band near 1189.4 cm^{-1} with a distinct Q-branch, as can be seen in Fig. 2. To determine the identity of this band, we can look at previous results in the far-IR. Zwart and Meerts observed two bands in their far-IR work, which they assigned as $\Pi(1_{10}) \leftarrow \Sigma(1_{01})$ and $\Pi(1_{01}) \leftarrow \Sigma(1_{01})$ [7]. Previous work with Ar–H_2O showed that the bending vibration is only slightly affected by the presence of the Ar atom in the complex [10], so we can estimate the locations of these bands in the infrared by simply adding the energy of the bending vibration to observed band origins observed in the far-IR. Doing this gives an estimated band origin of 1192.6 cm^{-1} for the $\Pi(1_{10}, v_2 = 1) \leftarrow \Sigma(1_{01})$ band (which is close to the actual band origin of 1192.87 cm^{-1} we report in Table 1) and 1189.5 cm^{-1} for the $\Pi(1_{01}, v_2 = 1) \leftarrow \Sigma(1_{01})$ band. This prediction lies only 0.1 cm^{-1} from the band presented in Fig. 2, leading us to assign this band as $\Pi(1_{01}, v_2 = 1) \leftarrow \Sigma(1_{01})$.

The presence of a strong Q-branch is consistent with this assignment, but we have not observed any P- or R-branch transitions associated with this band. A possible $R(0)$ line appears in Fig. 2 near 1189.59 cm^{-1}, but was also present in expansions using He as the carrier gas, indicating that the line is due to $(D_2O)_n$ clusters. The absence of P- and R-branch lines indicates that no transitions occur from the $\Sigma(1_{01})$ state to the $\Pi^e(1_{01}, v_2 = 1)$ state, which is in contrast to Zwart and Meerts [7], who observed P-, Q-, and R-branch transitions of this band in the far-infrared. The $1_{01}, v_2 = 1 \leftarrow 1_{01}$ transition in D_2O monomer is forbidden, and only occurs in Ar–D_2O because of mixing between the $\Pi(1_{01})$ and $\Pi(1_{10})$ states because of anisotropy in the potential energy surface of the complex [7]. It is unclear why only the $\Pi^f(1_{01}, v_2 = 1)$ would mix with the $\Pi(1_{10}, v_2 = 1)$ state, though the lack of P- and R-branch lines implies that this is the case. It is possible that the $\Pi^e(1_{01}, v_2 = 1)$ state does not mix because of Coriolis interaction with the $\Sigma^e(1_{01}, v_2 = 1)$ state.

We have fit the Q-branch transitions using the approach outlined above to obtain upper state constants, while keeping the constants for the $\Sigma(1_{01})$ state fixed to the values from Ref. [7]. The results are presented in Table 3 and a list of the observed transitions is presented in Table 4.

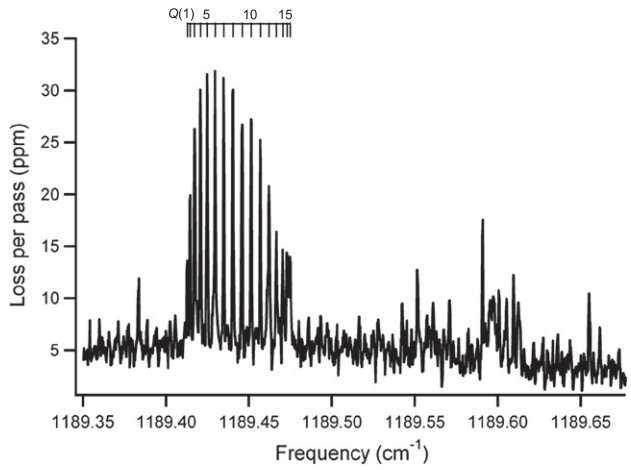

Fig. 2. Q-branch of the $\Pi(1_{01}, v_2 = 1) \leftarrow \Sigma(1_{01})$ band. The other lines present also appear in helium expansions and are not R-branch transitions, but are from $(D_2O)_n$ clusters. This spectrum was observed with ~700 Torr Ar backing pressure to improve signal-to-noise.

Table 3
Molecular constants (in cm^{-1}) for the $\Pi(1_{01}, v_2 = 1) \leftarrow \Sigma(1_{01})$ band and two newly observed $\Pi \leftarrow \Sigma$ bands. Values in parentheses represent one standard deviation from the least squares fit to the data. The labeling of the band 1 and band 2 constants as e or f assumes that the lower Σ state is an e state.

Parameter	$\Pi(1_{01}, v_2 = 1) \leftarrow \Sigma(1_{01})$	$\Pi \leftarrow \Sigma$ band 1	$\Pi \leftarrow \Sigma$ band 2
B''	0.09103344(33)[a]	0.0925124(86)	0.092491(16)
$D''(\times 10^6)$	1.7666(80)[a]	–	–
ν	1189.41215(11)	1191.584206(94)	1191.29042(18)
$B'(e)$	–	0.093026(13)	0.093050(15)
$D'(e)(\times 10^6)$	–	0.98(18)[b]	0.53(11)[b]
$B'(f)$	0.0914774(22)	0.0936565(87)	0.093601(17)
$D'(f)(\times 10^6)$	2.5568(85)	0.2924(32)[b]	0.273(24)[b]
σ	0.0002	0.0002	0.0003

[a] From Ref. [7].
[b] Reported values are actually ΔD because D'' was not included in the fit for these bands.

Table 4
Observed transitions for the $\Pi(1_{01}, v_2 = 1) \leftarrow \Sigma(1_{01})$ band (in cm^{-1}). Values in parentheses are residuals (observed – calculated) from the least squares fit.

Transition	Frequency
$Q(1)$	1189.4129(−2)
$Q(2)$	1189.4145(−3)
$Q(3)$	1189.4173(−1)
$Q(4)$	1189.4207(0)
$Q(5)$	1189.4249(1)
$Q(6)$	1189.4296(2)
$Q(7)$	1189.4348(2)
$Q(8)$	1189.4403(3)
$Q(9)$	1189.4459(2)
$Q(10)$	1189.4514(0)
$Q(11)$	1189.4569(−1)
$Q(12)$	1189.4621(−1)
$Q(13)$	1189.4665(−3)
$Q(14)$	1189.4704(−1)
$Q(15)$	1189.4730(−1)
$Q(16)$	1189.4748(3)

3.3. Additional $\Pi \leftarrow \Sigma$ bands

In addition to these bands we have observed two bands with clear P-, Q-, and R-branch structure near 1191.3 and 1191.6 cm^{-1}, as shown in Fig. 3. Both bands have an $R(0)$ transition and lack a $P(1)$ transition, identifying them as $\Pi \leftarrow \Sigma$ bands. These bands only appear at the relatively low backing pressures we used when collecting our spectra. As we increased the backing pressure of the supersonic expansion, the lines became progressively weaker until they disappeared altogether. As the backing pressure increases, the temperature of molecules in the expansion decreases, which suggests that these bands originate in excited internal rotor states in the ground vibrational state. As the temperature in the expansion decreases, these excited states will no longer be populated, leading to the decrease in signal. Because of this, it is not surprising that these bands were not observed by Li et al., because they used a backing pressure of ~4 bar in their expansion, which likely cooled all of the Ar–D_2O to the ground internal rotor states.

We have fit the two bands (which we refer to as band 1 for the stronger band at 1191.6 cm^{-1} and band 2 for the weaker band at 1191.3 cm^{-1}) using the approach outlined above and the results of the fit are presented in Table 3. The observed transitions are listed in Table 5. We excluded D'' from the fit for both bands because the uncertainty was larger than the constant when it was included. It is interesting to note that B'' for the two bands are nearly identical, which could be an indication that these two bands originate in the same lower state.

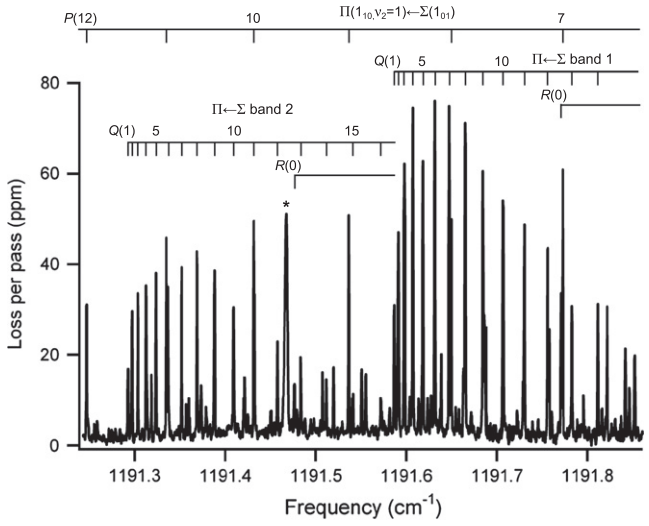

Fig. 3. Q-branch region of two previously unobserved $\Pi \leftarrow \Sigma$ transitions of Ar–D_2O between 1191 and 1192 cm^{-1}. The presence of $R(0)$ lines for both bands provide evidence that both are $\Pi \leftarrow \Sigma$ transitions. P-branch lines from the nearby $\Pi(1_{10}, v_2 = 1) \leftarrow \Sigma(1_{01})$ band can also be seen. The line marked with an asterisk (*) is due to HOD. Additional lines present in the spectrum are due to the presence of $(D_2O)_n$ clusters in the expansion. The spectrum was collected at a backing pressure of ~300 Torr.

Table 5
Observed transitions for the two newly observed $\Pi \leftarrow \Sigma$ bands (in cm^{-1}). Values in parentheses are residuals (observed – calculated) from the least squares fit.

Transition	Band 1	Band 2
$P(6)$	1190.4887(1)	
$P(5)$	1190.6687(−3)	1190.3766(1)
$P(4)$	1190.8501(0)	1190.5576(5)
$P(3)$	1191.0325(4)	1190.7381(−7)
$P(2)$		1190.9210(−6)
$Q(1)$	1191.5867(2)	1191.2926(0)
$Q(2)$	1191.5911(0)	1191.2970(0)
$Q(3)$	1191.5980(1)	1191.3036(−1)
$Q(4)$	1191.6070(0)	1191.3125(0)
$Q(5)$	1191.6183(0)	1191.3236(2)
$Q(6)$	1191.6314(−3)	1191.3367(2)
$Q(7)$	1191.6473(0)	1191.3518(1)
$Q(8)$	1191.6650(0)	1191.3687(−2)
$Q(9)$	1191.6844(−4)	1191.3883(2)
$Q(10)$	1191.7065(0)	1191.4091(−1)
$Q(11)$	1191.7304(3)	1191.4316(−6)
$Q(12)$	1191.7560(4)	1191.4576(6)
$Q(13)$	1191.7827(0)	1191.4833(−2)
$Q(14)$	1191.8115(0)	1191.5115(0)
$Q(15)$	1191.8419(0)	
$Q(16)$	1191.8738(0)	
$Q(17)$	1191.9069(0)	
$Q(19)$	1191.9764(−3)	
$Q(20)$	1192.0134(2)	
$R(0)$	1191.7707(4)	1191.4763(−3)
$R(1)$	1191.9574(1)	1191.6632(−6)
$R(2)$	1192.1453(0)	1191.8520(0)
$R(3)$	1192.3341(−1)	1192.0413(−1)
$R(4)$	1192.5240(1)	1192.2315(−1)
$R(5)$	1192.7140(−1)	1192.4231(2)
$R(6)$	1192.9051(1)	1192.6150(0)
$R(7)$		1192.8079(1)
$R(8)$		1193.0012(−1)

These two bands do not correspond to any transitions observed by far-IR spectroscopy of Ar–D_2O, and without further data it is difficult to definitively assign these bands. The observed bands could be due to transitions from low-lying internal rotor states of D_2O. There are two transitions of D_2O monomer that lie near this frequency range from low-lying rotational levels: 2_{02}, $v_2 = 1 \leftarrow 1_{11}$ at 1194.40 cm^{-1} and 2_{11}, $v_2 = 1 \leftarrow 2_{02}$ at 1193.26 cm^{-1} [20]. It is also possible that these bands both originate in the $n = 1$, $\Sigma(0_{00})$ intermolecular stretching state of Ar–D_2O.

To make a tentative assignment of these bands, we first consider the energies of the possible lower states compared to the ground $\Sigma(0_{00})$ state of Ar–D_2O. The $\Sigma(1_{11})$ state has been measured by far-IR spectroscopy to lie 20.7 cm^{-1} above the ground state [6], while the $\Sigma(2_{02})$ state is predicted to be ~32 cm^{-1} above the ground state according to the potential energy surface of Cohen and Saykally [13]. Cohen and Saykally also predicted that the intermolecular stretching state of Ar–D_2O lies ~36 cm^{-1} above the ground $\Sigma(0_{00})$ state. In a cold supersonic expansion, the lower-lying 1_{11} and 2_{02} states will be more populated than the intermolecular stretching state, making it more likely that we would observe transitions from these lower-lying states. In addition, the only transition from the intermolecular stretching state that might lie near this frequency region would be a red-shifted hot band transition of the $\Pi(1_{11}, v_2 = 1) \leftarrow \Sigma(0_{00})$ band observed near 1199 cm^{-1} (i.e., $\Pi(1_{11}, n = 1, v_2 = 1) \leftarrow \Sigma(0_{00}, n = 1)$) [12]. If we had observed this band, we would also expect to observe the $\Sigma \leftarrow \Sigma$ band instead of the two $\Pi \leftarrow \Sigma$ bands we have seen. Based on these arguments, we tentatively assign band 1 as $\Pi(2_{02}, v_2 = 1) \leftarrow \Sigma(1_{11})$ and band 2 as $\Pi(2_{11}, v_2 = 1) \leftarrow \Sigma(2_{02})$. The relative intensities of the bands support this assignment, as band 2 is weaker than band 1 and the 2_{02} level lies higher in energy than the 1_{11} level.

4. Conclusion

We have observed three previously unobserved bands of Ar–D_2O in the v_2 bend region of D_2O and provided additional data for the previously observed $\Pi(1_{10}, v_2 = 1) \leftarrow \Sigma(1_{01})$ band. We have fit all four bands using a pseudo-diatomic model for Ar–D_2O and obtained accurate excited-state molecular constants, as well as ground state constants for two of the new bands. We assign the band at 1189.4 cm^{-1} as the $\Pi(1_{01}, v_2 = 1) \leftarrow \Sigma(1_{01})$ band and tentatively identify two newly observed bands as $\Pi(2_{02}, v_2 = 1) \leftarrow \Sigma(1_{11})$ and $\Pi(2_{11}, v_2 = 1) \leftarrow \Sigma(2_{02})$, which have not previously been observed by microwave, far-infrared, or infrared spectroscopy.

Acknowledgments

The authors thank the group of Professor Claire Gmachl from the Electrical Engineering Department at Princeton University for providing the quantum cascade laser used for the present work. The development of our spectrometer has been supported by the NASA Laboratory Astrophysics Program and a David and Lucile Packard Fellowship. J.T.S. has been supported by a Robert C. and Carolyn J. Springborn Fellowship from the University of Illinois.

References

[1] G. Fraser, F. Lovas, R. Suenram, K. Matsumura, J. Mol. Spectrosc. 144 (1990) 97–112.
[2] T.C. Germann, H.S. Gutowsky, J. Chem. Phys. 98 (1993) 5235–5238.
[3] R.C. Cohen, K.L. Busarow, K.B. Laughlin, G.A. Blake, M. Havenith, Y.T. Lee, R.J. Saykally, J. Chem. Phys. 89 (1988) 4494–4504.
[4] R.C. Cohen, K.L. Busarow, Y.T. Lee, R.J. Saykally, J. Chem. Phys. 92 (1990) 169–177.
[5] R.C. Cohen, R.J. Saykally, J. Chem. Phys. 95 (1991) 7891–7906.
[6] S. Suzuki, R.E. Bumgarner, P.A. Stockman, P.G. Green, G.A. Blake, J. Chem. Phys. 94 (1991) 824–825.
[7] E. Zwart, W.L. Meerts, Chem. Phys. 151 (1991) 407–418.
[8] R. Lascola, D.J. Nesbitt, J. Chem. Phys. 95 (1991) 7917–7932.
[9] D.J. Nesbitt, R. Lascola, J. Chem. Phys. 97 (1992) 8096–8110.
[10] M.J. Weida, D.J. Nesbitt, J. Chem. Phys. 106 (1997) 3078–3089.
[11] D. Verdes, H. Linnartz, Chem. Phys. Lett. 355 (2002) 538–542.
[12] S. Li, R. Zheng, Y. Zhu, C. Duan, J. Mol. Spectrosc. 272 (2012) 27–31.

[13] R.C. Cohen, R.J. Saykally, J. Chem. Phys. 98 (1993) 6007–6030.
[14] J. Makarewicz, J. Chem. Phys. 129 (2008) 184310.
[15] B.E. Brumfield, J.T. Stewart, S.L. Widicus Weaver, M.D. Escarra, S.S. Howard, C.F. Gmachl, B.J. McCall, Rev. Sci. Instrum. 81 (2010) 063102.
[16] B.E. Brumfield, J.T. Stewart, B.J. McCall, J. Mol. Spectrosc. 266 (2011) 57–62.
[17] L. Rothman, I. Gordon, A. Barbe, D. Benner, P. Bernath, M. Birk, V. Boudon, L. Brown, A. Campargue, J.-P. Champion, K. Chance, L. Coudert, V. Dana, V. Devi, S. Fally, J.-M. Flaud, R. Gamache, A. Goldman, D. Jacquemart, I. Kleiner, N. Lacome, W. Lafferty, J.-Y. Mandin, S. Massie, S. Mikhailenko, C. Miller, N. Moazzen-Ahmadi, O. Naumenko, A. Nikitin, J. Orphal, V. Perevalov, A. Perrin, A. Predoi-Cross, C. Rinsland, M. Rotger, M. Šimečková, M. Smith, K. Sung, S. Tashkun, J. Tennyson, R. Toth, A. Vandaele, J. Vander Auwera, JQSRT 110 (2009) 533–572.
[18] C.M. Western, PGOPHER, a program for simulating rotational structure, 2010. <http://pgopher.chm.bris.ac.uk>.
[19] J.M. Hollas, Modern Spectroscopy, Fourth ed., John Wiley & Sons Ltd., Chichester, England, 2004.
[20] C. Camy-Peyret, J.M. Flaud, A. Mahmoudi, G. Guelachvili, J.W.C. Johns, Int. J. Infrared Milli. Waves 6 (1985) 199–233.